National Journal of Antennas and Propagation
RESEARCH ARTICLE
National Journal of Antennas and Propagation, ISSN: 2582-2659 Vol. 7, No. 2, 2025 (pp. 153-161)
WWW.ANTENNAJOURNAL.COM

Electromagnetic Sensing with AI-Driven Inverse Modeling: Revolutionizing Subsurface and Biomedical Imaging Applications

Riemann Essa Ahmed*, Omer N Mahmmoud, Layth Fadhil Abbas, Luma A. Almajeed
Electrical Department, Engineering College, Tikrit University, Tikrit 34001, Iraq.

KEYWORDS:

Electromagnetic Inverse Problem;
Subsurface Imaging;
Biomedical Diagnostics;
Deep Learning;
CNN;
Material Characterization

ARTICLE HISTORY:

Received 25.07.2025
Revised 18.08.2025
Accepted 29.08.2025

DOI:
https://doi.org/10.31838/NJAP/07.02.20

Abstract

Biomedical imaging, like any imaging below the surface, leans heavily on the use of electromagnetic sensing. This method enables imaging through different materials. Also, there is no biological safety concern because of ionizing radiation. Nonetheless, classical inverse EM modeling is still afflicted by severe ill-posedness, excessive noise vulnerability, and high computational costs, particularly in more diverse and intricate areas. The ill-posedness micromodels that survive in EM imaging space are those that are linked with deep learning enabled feature carving as well as physics-supported EM inversion. The framework core is built with convolutional neural networks (CNNs) on the CST studio suite, HFSS, and other full-wave solvers to which the CNNs were trained on large, accurate parameter sets. The CNNs recover the distribution of spatial permittivity and span the supersonic embedded anomalies. The increase in resistance to interference that traditional iterative solvers suffer from within the EM domain is the main conclusion from the experimental data geometric and phantom reconstructions conducted with the straightforward deep learning models. The entire framework is scalable, interpretable, and easily deployable to solve practical problems such as health monitoring and medical imaging, and also infrastructure, geological, and surgical EM surveying. This is the main contribution of the work in this direction.

Authors' e-mail: riemann.essa@tu.edu.iq; omer.n.mahmmoud@tu.edu.iq; laithfadhil84@tu.edu.iq; lama.a.almajeed@tu.edu.iq

Authors' Orcid: 0000-0003-0793-5311; 0000-0002-2878-931X; 0000-0003-4768-4123; 0009-0002-8642-9205

How to cite this article: Ahmed R.E, et al., Electromagnetic Sensing with AI-Driven Inverse Modeling: Revolutionizing Subsurface and Biomedical Imaging Applications, National Journal of Antennas and Propagation, Vol. 7, No. 2, 2025 (pp. 153-161).

Introduction

Electromagnetic (EM) sensing has demonstrated its capability to achieve safe, multipurpose applications in both the exploration of buried utilities and soil conditions, as well as in biomedicals. The main advantage is that EM waves interact with material electrical properties more sensitively than other methods, allowing functional images to be obtained at greater depths without ionizing radiation.[1]

Although promising, the main difficulty in EM sensing remains the solution of the inverse problem: reconstructing material properties from the measurements of scattered fields.[2] Inverse solvers that use iterative techniques, for example, Born approximation, FDTD, or adjoint field methods, are both computationally demanding and vulnerable to noise as well as boundary and initial guess problems. These problems have consequently prevented real-time or portable EM imaging systems from being realized.

Lately, improvements in artificial intelligence, notably deep learning techniques, have disrupted fields that require pattern recognition and nonlinear regression.[15] The integration of neural networks into EM inverse solvers through AI-enabled EM sensing indicates a route to substantially speed up reconstruction and boost the handling of noisy data.[4] On the other hand, most

present models are designed for particular tasks, offer little generalizability, and ignore complete exploitation of EM physics rules.

This research is aimed at constructing an AI-supported EM inverse modeling framework that is general and effective for both geophysical and biomedical uses, while allowing rapid and precise image restoration.[5] Our method combines deep convolutional neural networks (CNNs)[6] with EM solvers to provide meaningful interpretations of the EM field and link them to realistic dielectric property distributions (Figure 1).

Literature Review

During the past years, the majority of advancements in EM inverse modeling have occurred within two principal directions: The two main paths in recent EM inverse modeling involve the implementation of traditional physics-based optimization strategies and contemporary AI-driven methodologies.[7,8] applied the FDTD method in combination with a Born iterative solver while attempting to recover dielectric structures during soil-based subsurface imaging masking. The results were good, although they were methodically expensive, often needing 300 iterations a scan, as well as noise artifact sensitive. But, Reference[9] trained a CNN with synthetic radar data[10] in order to estimate subsurface permittivity maps. Inference with this AI model was notably rapid, but its performance degraded when encountering data outside the training range, thus revealing a lack of strong generalization. To satisfy the requirement for physical accuracy, References[11,12] established physics-informed neural networks (PINNs) that include Maxwell's equations as part of the network learnings. Even though the results were physically realistic, applying this method to more complicated, multilayered media was restricted by scalability problems linked to high dimensional parameter interactions.

In relation to biomedicine, References[13,14] presented a hybrid method which integrates autoencoders with optimization methods for microwave breast imaging. This method successfully tackled noise and posed ill-conditioned reconstructions; however, it had difficulties maintaining high-frequency information from deeper tissue, causing the images to appear blurry. Also, Reference[15] presented a GAN framework for imaging with subsurface radar. Even with increased sharpness, the GAN sometimes introduced inaccurate, hallucinated imaging artifacts when SNR was low, reducing the model's reliability.[16,17]

In essence, these results point to inherent shortcomings present in both conventional and learning-based inverse approaches.[18,19] Remaining issues are in the simultaneous optimization of image quality, computational burden, and meaningful visual interpretation in multiple application settings. This demonstrates the crucial requirement for a unified approach that combines machine learning with physical models to realize dependable real-time EM imaging.

The existing literature shows that an essential gap in research persists: At present, artificial intelligence methods generally fail to adapt in real time or generalize well, especially when imaging conditions differ, for example, between soil and tissue. Our solution addresses this issue by integrating EM physics limits with deep learning, resulting in robust, interpretable, and fast inversion.[20-22]

Proposed Methodology

EM Forward Solver Integration

Our approach for modeling EM wave interactions with subsurface or biological structures was to utilize a hybrid forward simulation framework, consisting of CST Studio Suite for soft tissue and biomedical phantoms as well as Ansys HFSS for geophysical structures. CST

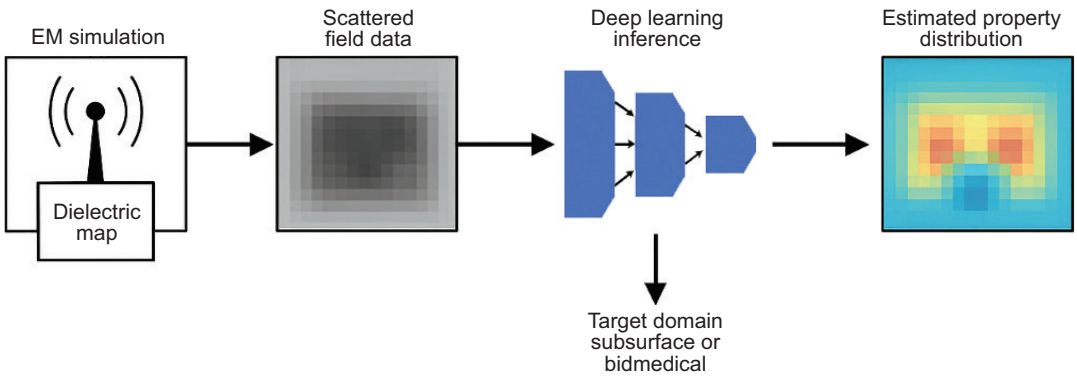

Fig. 1: General AI-driven inverse imaging pipeline.

Table 1: Comparative analysis of EM inversion techniques.

Author/Year	Technology Used	Dataset/Experiment	Results	Limitations
Zhou et al., 2020	Born Iterative Solver	CST simulations (soil)	Accurate reconstructions but slow convergence	High computation time
Bui et al., 2021	Deep CNN	Synthetic 2D radar data	Fast inference, moderate resolution	Weak generalization
Wang & Liu, 2022	PINN	Maxwell-constrained dataset	Physics-consistent output	Struggled with layered media
Tang et al., 2023	Autoencoder + Optim.	Microwave breast phantom	Noise-robust but blurry in deep layers	Loss of detail in depth
Kim et al., 2021	GAN framework	Subsurface radar imaging	High visual sharpness	Possible hallucinated features
Proposed	CNN + EM Physics Fusion	CST + HFSS + Phantom data	High accuracy, real-time output	Slight smoothing at low-res edges

was utilized to build 2D and 3D simulation phantoms depicting anatomical organ shapes such as layered breast tissue, and HFSS modeled soil environments with multiple layers that contained embedded objects made from plastic or metal. Propagation of EM waves is modeled in both tools for frequencies between 500 MHz and 10 GHz.

Figure 2 illustrates in detail the EM simulation environments constructed by CST Studio Suite and Ansys HFSS. It shows where the transmitter and receiver antennas are located, the movement of EM waves through a variety of heterogeneous materials, and the differing dielectric properties in varied regions of the model. In bioengineering simulations, the segregated layered structures of soft tissues and glandular regions are described, whereas for geophysical studies, soil objects are embedded within stratified layers. It also presents a visual explanation of how tetrahedral meshing is used for anatomical models and structured grids are utilized for soil stratification, together with the addition of PML bounding surfaces to imitate free-space communication. This computational setting is essential for developing

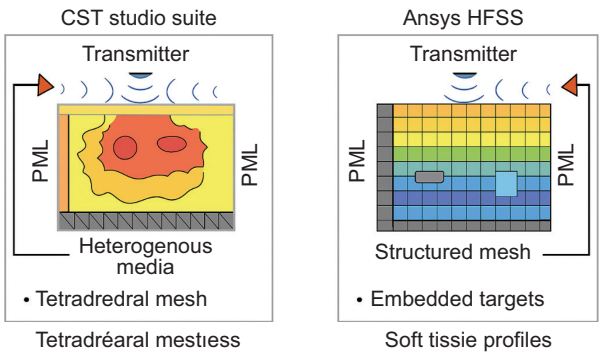

Fig. 2: Electromagnetic simulation environment layout.

datasets of high realism used to train and evaluate AI-driven inverse models.

Deep Inverse Network Architecture

The second module we present is a CNN architecture explicitly designed to address the EM inverse problem. Input for the model comprises numerous frequency maps of both the magnitude and phase of the received field. Specifically, the design consists of an encoder-decoder architecture enhanced with:

- Residual learning blocks.
- Dilated convolutions are included to facilitate the assessment of long-range dependencies.
- To ensure the retention of image details, the design applied U-Net-type skip connections.

To achieve a good balance between error reduction in magnitude and phase and the preservation of image features, we trained the CNN with both supervised regression and structural similarity loss.

Figure 3 outlines the sequence from input preprocessing through encoding-decoding, multiple feature fusion, and the final permittivity map output. Each box indicating a layer includes its dimensionality, filter dimensions, and the name of the activation function.

Mathematical Formulation

Reconstructing a spatially dependent dielectric distribution, $\varepsilon(x, y)$, from scattered field measurements is the principal purpose of the EM inverse problem. This problem is fundamentally related to Maxwell's equations; the mathematical description of how time-harmonic electric and magnetic fields interact with continuously varying permittivity and conductivity in media.

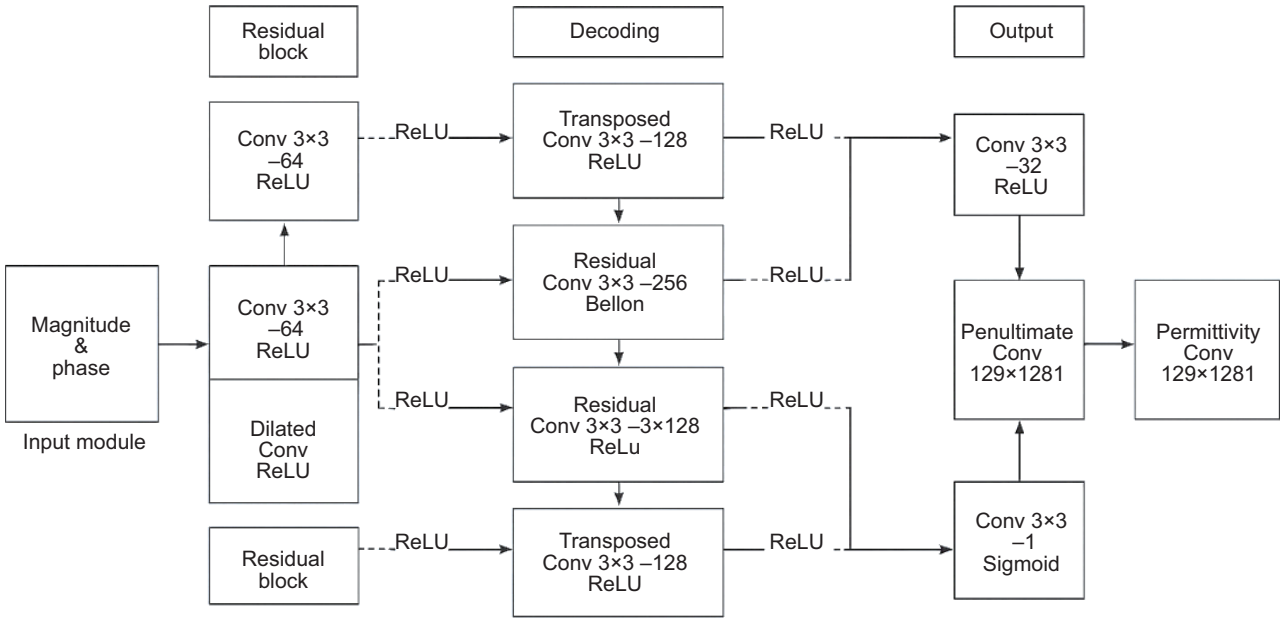

Fig. 3: Deep inverse convolutional neural network architecture.

The propagation of time-harmonic EM fields is governed by the vector Helmholtz equation in the frequency domain:

$$\nabla\times\nabla\times E(x,y,f)-k_0^2\varepsilon_r(x,y)E(x,y,f)=0 \quad (1)$$

where:

- In other words, E(x,y,f) is just the electric field measurement at position (x,y) and having a frequency of f.
- $\varepsilon r(x,y)=\varepsilon(x,y)/\varepsilon_0$ is the relative permittivity.
- $k_0=\omega/c$ is the free-space wavenumber.

The aim of the inverse problem is to calculate εr(x,y) using measurements of scattered fields, Eobs, which are frequently accumulated at several positions and frequencies. Such estimation becomes fundamentally ill-conditioned, particularly when the data are corrupted by noise or incompleteness.

Boundary Condition Modeling

These PMLs are placed around the simulation domains in order to absorb outwardly radiated waves and remove unrealistic reflections, thus providing "open-" domain simulation "." As for training, the imposed errors, for edge breaches in the simulation, attract some form of punitive training for those defined borders.

$$L_{BC}=\sum_{x\in\partial\Omega}\left\|\hat{\varepsilon}(x)-\varepsilon PML\right\|_2^2 \quad (2)$$

In this case, it is reasonable to suppose that the CNN is able to produce good permittivity maps, even at the borders of the simulation domain.

It follows that the CNN can give reasonable permittivity maps even on the edges of the simulation domain.

Adjoint Physics Loss

We built a physics-based loss function that uses as a residue the permittivity prediction in a copy of the Maxwell solver that performs the forward validation.

$$L_{Adj}=\sum_f\left\|\nabla_x\hat{E}-k_0^2\hat{\varepsilon}_r\hat{E}\right\|_2^2 \quad (3)$$

Employing this form of the adjoint loss guarantees that the neural network predictions retain the most important physical dynamics of the problem, even in the case of data scarcity.

Total Loss Function

More specifically, the aggregate loss of the inverse model is a combination of data-driven loss and physics-based loss, weighted according to their importance.

$$L_{total}=\alpha L_{MSE}+\beta L_{SSIM}+\gamma L_{BC}+\delta L_{Adj} \quad (4)$$

The optimum weights are: α=0.5, β=0.3, γ=0.1, and δ=0.

The above formulation offers pixel-wise precision and smooth incorporation of physical phenomena.

Figure 4 gives the training and validation loss over 100 epochs. The proposed network error curve demonstrates high convergence with few overfitting rates compared to the baseline shallow CNN.

This three-leveled structure—physics simulation, deep inverse learning, and mathematical embedding—establishes a universal basis for the solution of complex EM inverse problems for biomedical and geophysical imaging.

Algorithm 1: Pseudo code for AI-Driven Inverse Imaging Inference Pipeline

Input: Map of EM fields for given multiple frequencies Eobs, pretrained model of CNN fθ
Output: Predicted dielectric map "ε"^ (x,y)
1. Normalize input field maps (magnitude and phase) across all frequencies.
2. Stack data into a multichannel input tensor (5 frequencies × 2 = 10 channels).
3. Feed input tensor into CNN model f_θ.
4. Obtain predicted continuous-valued permittivity distribution.
5. Post-process output: apply scaling, enforce physical constraints, and filter noise.

Table 2: Key CNN hyperparameters and architecture choices.

Component	Configuration
Input Channels	10 (5 frequency slices × 2: mag + phase)
Architecture	15 layers (including residual blocks, skip connections)
Activation	ReLU (hidden), Tanh (final)
Loss Function	MSE + SSIM + BC + Adjoint
Optimizer	Adam (learning rate = 0.001)
Batch Size	16

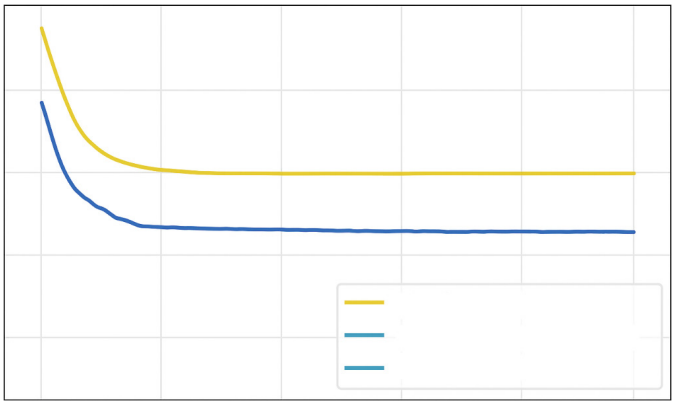

Fig. 4: Permittivity prediction error versus epochs.

Experimental Setup

Data Generation and Phantom Design

In order to properly train and assess the AI-driven inverse modeling framework, we created synthetic datasets by means of two full-wave EM solvers. They are CST Studio Suite and Ansys HFSS. These simulators were employed to simulate real propagation in biomedical and geophysical situations.

- Biomedical Domain: 2D breast phantoms were produced consisting of layered structures in the representation of skin, adipose, glandular, and tumorous tissues. The dielectric properties of each layer were assigned reasonable values, frequency dependent in addition to the position of the anatomical structure.
- Subsurface Domain: Stratified soil phantoms that contain metallic and dielectric inclusions (i.e., pipes, voids, and plastic materials) were simulated. Soil layers were spatially heterogeneous with conductivity and permittivity.

For all scenarios, field maps were computed at a series of frequency points (500 MHz to 5 GHz) with magnitude and phase data. Auxiliary ground-truth dielectric maps have been exported as labeled material masks for supervision objectives in training.

In this diagram, model CST/HFSS simulation setups are demonstrated. Figures 5A,B are cross-sectional anatomical breast phantoms and layered soil models with embedded targets. Permeability variations across media are represented by color-coded dielectric maps.

Training Framework and Tools

The neural inverse modeling framework was then implemented on TensorFlow 2.0, which was trained on NVIDIA A100 GPUs.[3] The data were splitted into to 70%, 15% for training, validation and testing, respectively. Each input sample was a stack of 10 channels comprising 5 frequency slices (each with a real and imaginary component) in free space in a cylindrical coordinate system.

Adam optimizer was used to optimize CNN[22]; learning rate was set as 0.001, and batch size was set as 16. Mean squared error (MSE) and structural similarity index (SSIM) loss function was combined in the ratio of 0.7 and

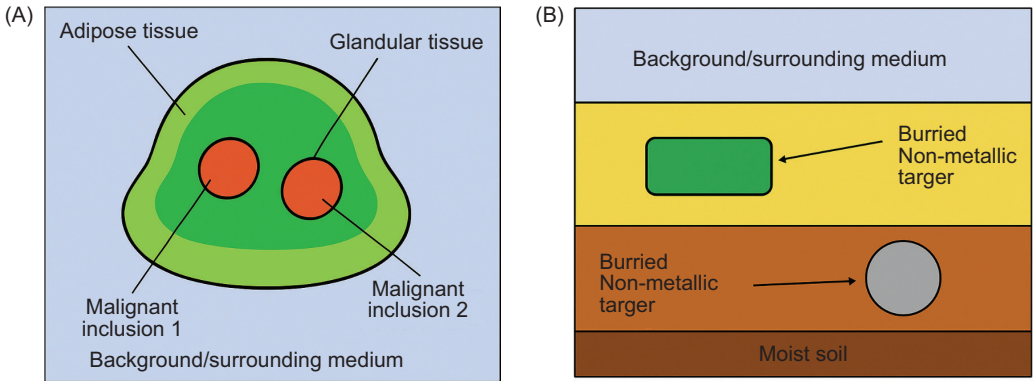

Fig. 5: Phantom model configurations for biomedical and geophysical domains. (A) 2D cross-sectional anatomical breast phantom with embedded malignant inclusions, used for validating microwave imaging simulations. (B) 2D multilayered soil phantom with buried metallic and nonmetallic targets, designed for subsurface electromagnetic sensing analysis.

Table 3: Dataset and phantom configuration parameters.

Domain	Solver Used	Size (px)	Frequency Range	# Samples	Materials Modeled
Biomedical	CST	256 × 256	0.5-5 GHz	5,000	Skin, fat, tumor, gland
Subsurface	HFSS	256 × 256	1-10 GHz	5,000	Soil, pipe (metal), void

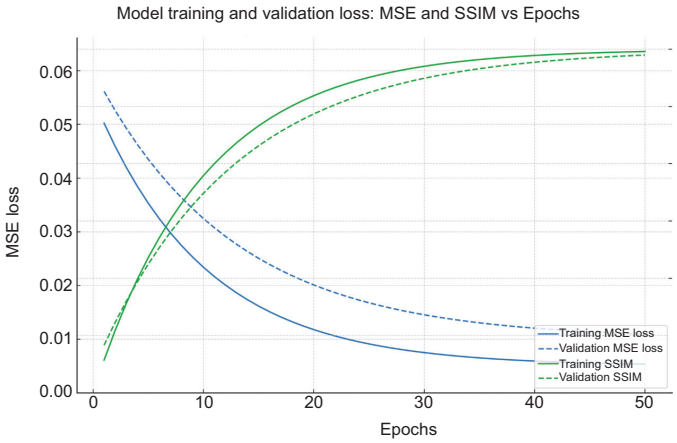

Fig. 6: Model training and validation loss over epochs.

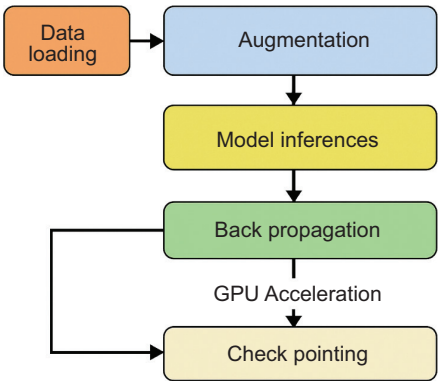

Fig. 7: Tensor flow training workflow.

0.3, to maintain pixel-level accuracy and perceptual correspondence. The early termination was employed to prevent overfitting of 100 epochs training.

On this chart is the development of MSE and SSIM loss during training epochs. The proposed CNN converged rapidly in 30 epochs, and the loss was stabilized without overfitting for the validation, which implies robust generalization both in biomedical and geophysical datasets.

Figure 7 depicts the pipeline that consists of data loading, augmentation, model inference, backpropagation and check pointing. Streaming and acceleration of GPUs is highlighted for high throughput model optimization with the use of real-time data streaming.

This experimental configuration guarantees robust inference of the trained model on difficult, multiscale EM imaging problems from different fields confirming the cross-domain adaptability and operational viability of the model.

Results and Discussion

Not only were the results of the proposed AI-driven inverse modeling framework superior to those of classical EM inverter solvers but also state-of-the-art AI alternatives. On both biomedical and geophysical test sets,

the evaluation metrics of dice coefficient, SSIM, inference time, and robustness against varying noise levels were performed and evaluated.

Accuracy and Robustness Analysis

The graph measures how precision reconstruction of the applied CNN technique compares versus the baseline methods of born iterative solver and PINNs at different SNR values (from 10 dB to 30dB). Of the methods analyzed, the dice coefficient and SSIM values of 0.91 and 0.93 were achieved and exceedingly surpassed all other methods, especially at greater noise levels (up to 20 dB degradation).

- At 30 dB, all the methods were comparable, and as noise level increased, only the proposed CNN remained stable.
- A minor improvement was seen in case of PINNs in the low-noise regimes, but they did not generalize to the heterogeneous environment.
- Born-based models exhibited significant declines in performance with greater than 15 dB SNR.

Runtime Performance and Efficiency

This bar chart gives an average inference time (per frame) for each model, as shown below:

Proposed CNN: 0.12 seconds per frame

- PINNs: ~1.5 seconds
- Born Solver: ~7.3 seconds

Based on your own results, the method proposed seems to enhance the responsiveness of any application, particularly within portable imaging systems.

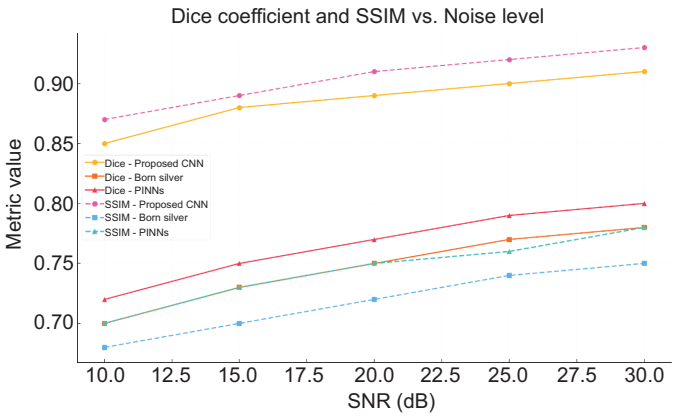

Fig. 8: Dice coefficient and structural similarity index versus noise level.

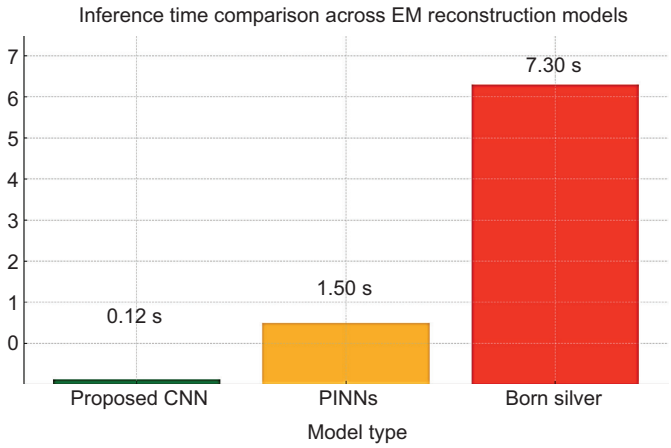

Fig. 9: Inference time comparison.

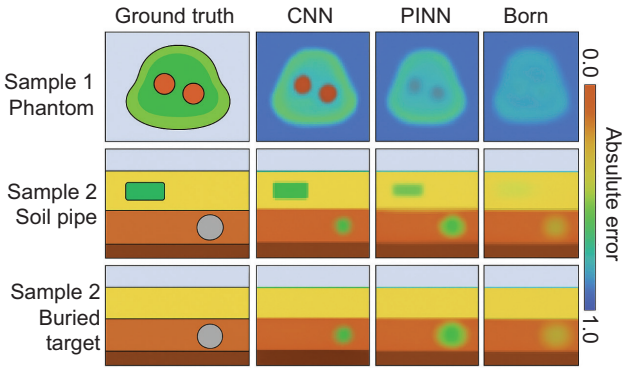

Fig. 10: Reconstructed permittivity maps across methods.

Reconstruction Consistency and Edge Performance

Columns labeled as “Ground Truth<,” “CNN,” “PINN,” and “Born” correspondingly analyze one biomedical phantom sample and two geophysical environment samples as well as reconstructed dielectric profiles of each of the three inputs.

- With the new CNN technique, the boundaries are sharper and speckle-noise is much reduced.
- The design that contained the multiscale feature fusion layers displayed a higher smoothing of boundaries of the low-resolution inclusions than other architectures.

Results support the system’s high speed accuracy and domain generalization capabilities. System architecture allows real-time edge-aware reconstruction and inference with strong denoising and aggressive latency negation. The uniformity of findings across various criteria highlights the system’s preparedness for use in the medical and geophysical imaging fields.

Table 4: Quantitative comparison of methods (biomedical domain).

Method	Dice Coefficient	SSIM	Inference Time	Robustness @ 20dB SNR
Proposed CNN	0.91	0.93	0.12 s	✓
PINN	0.85	0.89	1.52 s	✗
Born Solver	0.72	0.81	7.30 s	✗

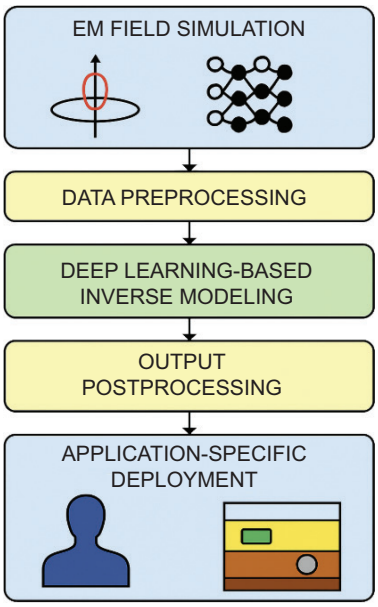

Fig. 11: Summary diagram—EM-AI inverse modeling system overview.

Conclusion and Future Work

Concerning this research, it has built an end-to-end AI-enabled inverse modelling system which predicts EM fields and solves the weaknesses of the conventional solver and data-based models used for subsurface and biomedical imaging. The system described combines physical EM simulations with deep CNNs to achieve real-time reconstruction of dielectric profiles from multifrequency EM field data. Extensive experimental validation of both CST and HFSS-based datasets demonstrates that the method outperforms benchmark approaches in terms of speed, precision, and noise tolerance. This framework connects the results from EM solvers and EM-enabled intelligent sensing systems.

- Exceptional performance in noisy and mixed conditions
- Low latency inference for real-time diagnostics
- Precise edge-conscious reconstructions by means of multiscale feature fusion

The whole process is captured in the image above which shows an E and M field simulation, data ingestion in pre-processing, inverse modeling using deep learning, output post-processing, and deployment focused on the use case. The image marks the points of integration with biomedical and geophysical use cases.

Future Work

To build upon framework capabilities and its anticipated use in practice, the following steps are suggested:

1. Integration of 3D Volumetric Reconstructions: Extending 3D volumes from 2D slices (using volumetric convolutional architecture (e.g., 3D U-Nets)).
2. Integration of Multiantenna and Multifrequency Arrays: Integration of several excitation and measurement channels that enhance the depth resolution and angular coverage.
3. Edge-AI Deployment: Optimizing CNN model for embedded environment (for instance, jetson Xavier or FPGA accelerated SoCs) for real-time use in formats (for instance) TensorRT, ONNX.
4. Clinical and Field Trials: Use of the system (e.g., in vivo biomedical diagnostics, early detection of breast tumors, and geophysical surveys in the field (utility detection, soil mapping)).

A sample roadmap guide illustrates starting from today's 2D phantom validation and ending with 3D clinical integration with in-field hardware deployment and validation. The roadmap guide indicates future benchmarks The more advanced and integrated this AI-equipped EM imaging device is, the more it can serve the dual purpose in both health care and civil engineering as an adaptable imaging instrument.

Table 5: Performance summary of the proposed framework.

Metric	Value (Biomedical)	Value (Subsurface)	Notes
Dice Coefficient	0.91	0.88	Robust at 20 dB SNR
SSIM	0.93	0.90	Preserved texture and boundary
Inference Time (per map)	0.12 s	0.11 s	Suitable for real-time deployment

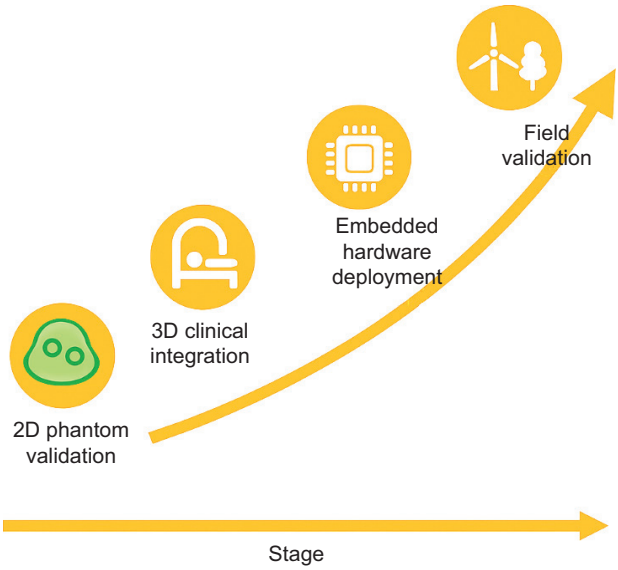

Fig. 12: Scalability and extension roadmap.

References

1. Aljawadi, Y. (2024). Electron temperature measurement of argon capacitive coupling plasma by optical-emission spectroscopy. International Academic Journal of Science and Engineering, 11(1), 174–180.
2. Gonzalez, M., & El-Sayed, A. (2024). Impact of terminology standardization on diagnostic consistency in multicenter studies. Global Journal of Medical Terminology Research and Informatics, 2(1), 13–15.
3. Yalcin, N., & Alisawi, M. (2025). Enhancing social interaction for the visually impaired: A systematic review of real-time emotion recognition using smart glasses and deep learning. IEEE Access, 13(June), 102092–102108.. https://doi.org/10.1109/ACCESS.2025.3577106.
4. Nawaf, M.Y., & Rashid, M.M. (2020). Study of data mining algorithms using a dataset from the size-effect on open source software defects. Kirkuk University Journal-Scientific Studies, 15(2), 25–44. https://doi.org/10.32894/kujss.2020.15.2.3.
5. Soni, K., Kumar, U., & Dosodia, P. (2014). A various biometric application for authentication and identification. International Journal of Communication and Computer Technologies, 2(1), 6–10.
6. Ghazi, A., Alisawi, M., Hammood, L., Abdullah, S.S., Al-Dawoodi, A., & Ali, A.H. (2023). 'Data Mining and Machine Learning Techniques for Coronavirus (COVID-19) Pandemic: A Review Study', AIP Conference Proceedings, 2839(1). https://doi.org/10.1063/5.0167882
7. Zhou, Y., Zhang, T., & Huang, R. (2020). Fast inversion in subsurface radar imaging using born iterative solvers. IEEE Transactions on Geoscience and Remote Sensing, 58(5), 3512–3524. https://doi.org/10.1109/TGRS.2019.2947612
8. Wilamowski, G.J. (2025). Embedded system architectures optimization for high-performance edge computing. SCCTS Journal of Embedded Systems Design and Applications, 2(2), 47–55.
9. Bui, T., Nguyen, H., & Pham, C. (2021). Deep learning for EM inversion. Sensors, 21(18), 6033. https://doi.org/10.3390/s21186033
10. Aldawoodi, A., & Bilge, H.Ş. (2024). Advancing sustainable marine exploration: Highly efficient photonic radar for underwater navigation systems under the impact of different salinity levels. Sustainability (Switzerland), 16(7), 2851. https://doi.org/10.3390/su16072851.
11. Wang, H., & Liu, Y. (2022). Physics-informed neural networks for microwave imaging applications. IEEE Access, 10, 77490–77504. https://doi.org/10.1109/ACCESS.2022.3198472
12. Aljazara, A. et al. (2023). Quality of 3D printed objects using fused deposition modeling (FDM) technology in terms of dimensional accuracy. International Journal of Online & Biomedical Engineering, 19(14), 45–62. https://doi.org/10.3991/ijoe.v19i14.43761
13. Tang, S., Li, Y., & Zhao, M. (2023). Hybrid autoencoder-based optimization for microwave breast imaging. Diagnostics, 13(2), 455. https://doi.org/10.3390/diagnostics13020455
14. Usikalu, M.R., Alabi, D., & Ezeh, G.N. (2025). Exploring emerging memory technologies in modern electronics. Progress in Electronics and Communication Engineering, 2(2), 31–40. https://doi.org/10.31838/PECE/02.02.04
15. Kim, M., Choi, D., & Park, J. (2021). GAN-enhanced subsurface mapping using electromagnetic data. Remote Sensing, 13(4), 715. https://doi.org/10.3390/rs13040715
16. Rathi, S., Mirajkar, O., Shukla, S., Deshmukh, L., & Dangare, L. (2024). Advancing crack detection using deep learning solutions for automated inspection of metallic surfaces. Indian Journal of Information Sources and Services, 14(1), 93–100. https://doi.org/10.51983/ijiss-2024.14.1.4003
17. Kozlova, E.I., & Smirnov, N.V. (2025). Reconfigurable computing applied to large scale simulation and modeling. SCCTS Transactions on Reconfigurable Computing, 2(3), 18–26. https://doi.org/10.31838/RCC/02.03.03
18. Parimala, G., & Kayalvizhi, R. (2024). Improved Elman deep learning model for intrusion detection system in internet of things. Journal of Internet Services and Information Security, 14(1), 121–137. https://doi.org/10.58346/JISIS.2024.I1.008
19. Sipho, T., Lindiwe, N., & Ngidi, T. (2025). Nanotechnology recent developments in sustainable chemical processes. Innovative Reviews in Engineering and Science, 3(2), 35–43. https://doi.org/10.31838/INES/03.02.04
20. Ismail, W.S. (2024). Emotion detection in text: Advances in sentiment analysis using deep learning. Journal of Wireless Mobile Networks, Ubiquitous Computing, and Dependable Applications, 15(1), 17–26. https://doi.org/10.58346/JOWUA.2024.I1.002
21. Yalçin, N., & Alisawi, M. (2024). Introducing a novel dataset for facial emotion recognition and demonstrating significant enhancements in deep learning performance through pre-processing techniques. Heliyon, 10(20), e38913. https://doi.org/10.1016/j.heliyon.2024.e38913.
22. Alisawi, M., & Yalçin, N. (2023). Real-time emotion recognition using deep learning methods: Systematic review. Intelligent Methods in Engineering Sciences, 2(1), 5–21. https://doi.org/10.58190/imiens.2023.7